

# HIGH CURRENT ION SOURCES, BEAM DIAGNOSTICS AND EMITTANCE MEASUREMENT

M. Cavenago\*, M. Comunian, E. Fagotti, M. Poggi, INFN-LNL, Legnaro, Italy  
T. Kulevoy, S. Petrenko, INFN-LNL, Legnaro, Italy and ITEP, Moscow, Russia

## Abstract

Singly charged ion sources can easily surpass the 1 kW beam power, as in TRIPS ( $H^+$ , 60 mA, 80 kV, now installed at LNL) or in NIO1 ( $H^-$ , 130 mA distributed into 9 beamlets, 60 kV, a project of RFX and INFN-LNL). Beam diagnostic constitutes an important instrument in the high current source development. Even if calorimetric and optical beam profile monitors become possible, still a phase space plot of the beam will be the most useful tool for validation of extraction simulation and for input of subsequent beam transport optimization. Improvements in extraction beam simulations are briefly reported, and effect of space charge neutralization is discussed. Since preliminary design of the traditional two moving slit beam emittance meter show problems with slit deformations and tolerances and with secondary emission, an Allison scanner was chosen with the following advantages: only one movement is needed; data acquisition is serial and signal can have an adequate suppression of secondary electrons. The design of a compact Allison scanner head is discussed in detail, showing: 1) the parameter optimization; 2) the segmented construction of electrodes. Experimental commissioning at lower power seems advisable.

## INTRODUCTION

An ion source extraction system requires careful design, its difficulty generally increasing with the beamlet perveance ( $I_b V_b^{-3/2}$ ) [1] and the nucleon number  $A$  of the dominant ion species and the number  $N$  of beamlets; here  $V_b$  is the source acceleration voltage and  $I_b$  the current per beamlet. The worldwide effort to improve ion sources, mainly for fusion application, requires detailed modeling of the plasma depending on several parameters (namely the plasma potential, the negative ion to electron ratio) difficult to measure directly. A high quality emittance measurement will be crucial to validate most code and plasma modeling, and to reliably design the following beam line; it is a topic of the NIO2BEAM experiment (financed by INFN-CSN5). An emittance meter design based on an Allison scanner is described in this paper.

Use of negative ions in high current sources is related to need of having a charge exchange (CX) later, to accumulate more beam in a given phase space or to enter a high magnetic field as a neutral beam; CX cross section (over few hundred keV) favours negative ions over positive ions; in other words, negative ions are more difficult to produce,

\*cavenago@lnl.infn.it

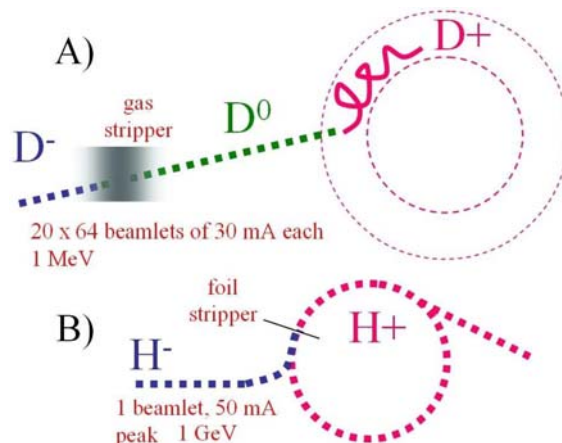


Figure 1: Typical applications of high current negative ion sources: A) Tokamak injection (40 MW average) is a two stage gas stripping: the second stripping happens inside tokamak plasma. A gas target (called the neutralizer) is used for the first stripping. Beam emittance is determined by  $D^-$  source; B) Spallation Neutron Source (1.4 MW average).

hence they are easier to dismount. Typical applications (see Fig. 1) are the neutral beam injectors (NBI), featuring 1280 beamlets of 35 mA each of  $D^-$  for the ITER project (2 or 3 NBI needed) and the Spallation Neutron Source (single beam, 65 mA of  $H^-$ ) [2, 3, 4]. In other applications, where no beam accumulation is needed, positive ions are obviously preferred (IFMIF project, two beams of 125 mA each of  $D^+$  [5]). Beam extracted from  $D^+$  sources can be generally contaminated by  $D^{2+}$  and  $D^{3+}$  molecular ions.

Gas filling pressure of the source  $p$  is typically in the range from 0.3 to 3 Pa, while higher pressures are found in industrial ion sources. Negative ion formation inside the source requires two plasma regions, separated by a so called magnetic filter. In the first region, radiowaves with frequency  $f_1$  heat an inductively coupled plasma (ICP) to a temperature  $T_{1e} \geq 4$  eV, which is determined from global plasma balance laws [6], to produce a reasonable rate of dissociation of molecular hydrogen. In some prototypes, plasma heating was obtained by an arc discharge with voltage  $\cong 100$  V between filaments and the source chassis; in industrial sources, rf voltage is applied to an electrode (so to have a capacitively coupled plasma, CCP). Note that we measure plasma temperature in energy unit, that is to say that  $T$  should be read  $k_B T_K$  where  $k_B$  is the Boltzmann constant and  $T_K$  is the standard temperature (in Kelvins).

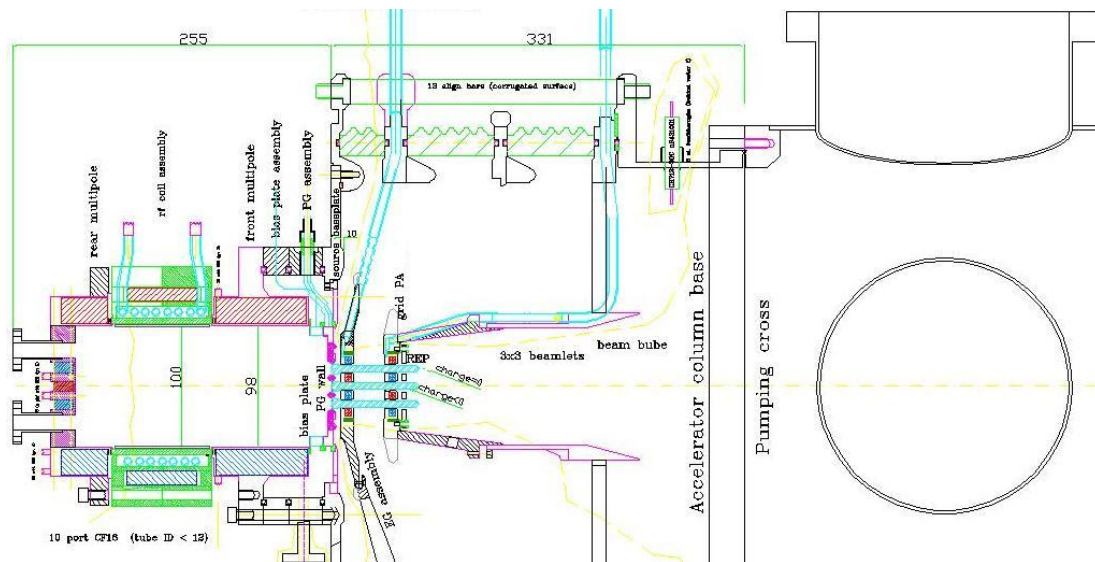


Figure 2: A view of NIO1 design. Scanner(s) can fit into the CF200 ports shown, or in similar ports spaced each 0.5 m.

The second plasma region (near the plasma grid electrode PG) must have a small enough electron temperature  $T_{2e}$  to reduce the ionization of  $H^-$ , which has an electron affinity of 0.753 eV. To fix ideas  $T_{2e} \cong 1$  eV; negative ions can be produced by dissociative attachment to a vibrationally excited  $H_2$  molecule (produced in the first region) or by collisions of fast H atoms (always produced in the first region) with cesium atoms adsorbed on the PG wall. A third production mechanism consider that vibrationally excited  $H_2$  molecule can be also produced efficiently by impact of fast particles on the PG walls [7].

In positive ion sources (based on rf or filament) we still find a magnetic filter, which has the purpose of reducing the fraction of  $H_3^+$  in the extracted beam [8]. Moreover, in both sources most of the metallic walls are covered by magnetic multipoles [1], to reduce plasma energy loss. Other positive ion sources (like TRIPS built at LNS and now installed at LNL [9]) are based on microwaves and higher magnetic fields [10], around the well-known electron cyclotron resonance (ECR)

$$\omega_c(\mathbf{x}) = eB(\mathbf{x})/m_e\gamma = \omega \quad (1)$$

where  $\omega = 2\pi f_1$ . TRIPS uses a 80 kV extraction voltage for extracting a 50 mA beam from a 6 mm hole; the extraction system is a pentode, with electrode voltages of +80 kV, +35 kV, 0, -2.5 kV, 0 (listed with increasing  $z$ ) with respect to ground.

Important advantages of ICP sources with an external rf coil and of ECR sources are the absence of arcs inside the plasma and a longer duration. Moreover, it can be speculated that ICP can achieve a larger power efficiency than filament or CCP sources; up to now, the need to use a so called Faraday shield (to protect alumina parts from plasma heat load) has hindered this goal. In the source NIO1 (Negative Ion Optimization phase 1) under development at Consorzio RFX and INFN-LNL, permanent magnets may be

placed also behind the alumina walls, so to test operation without Faraday shield.

A plan of NIO1 is shown in Fig. 2 [11]. The nine beamlets are arranged into a  $3 \times 3$  square matrix, so that electrodes can be rotated by 90 degrees during assembly. Source is made from five modules, the rear multipole, the rf coil assembly, the front multipole (with a filter magnet submodule), the bias plate assembly and the PG assembly. The extraction column is basically a triode, made of the PG, the extraction grid EG and the acceleration grid PA; actually PA may be floated by a small positive voltage with respect to the following drift tube at ground potential, to improve the space charge compensation of the drifting beam; nominal voltages are  $\phi_{PG} = -60$  kV,  $\phi_{EG} = -52$  kV,  $\phi_{PA} = 0.15$  kV with respect to the following drift tube at  $\phi = \phi_{dr} = 0$ . A small repeller electrode REP may be inserted before the drift tube; in that case nominal voltages are  $\phi_{REP} = 0.15$  kV and  $\phi_{PA} \cong \pm 0.01$  kV.

## SPACE CHARGE EFFECTS

The Poisson equation is

$$\Delta\phi = -\rho/\epsilon_0 = -(e/\epsilon_0)[N_p - N_n - N_e] \quad (2)$$

with  $N_p$  the density of positive ions (times the their average charge state  $\bar{i}_p$  in general),  $N_n$  the density of negative ions and  $N_e$  the electron density; in our case  $\bar{i}_p = 1$ . These densities are to be related to  $\phi$ .

Some approximation may be valid in particular plasma or beam regions, like the Maxwellian density  $N_p \propto e^{-\phi}$  for ions trapped into the plasma or  $N_n \propto (\phi - \phi_{pl})^{-1/2}$  in the so called free fall regimes [12], as in a planar collisionless acceleration; here  $\phi_{pl}$  is the plasma potential (near to  $\phi_{PG}$ ) whose exact definition is model dependent. Simulating these regions with standard multiphysics tools [13] is then straightforward.

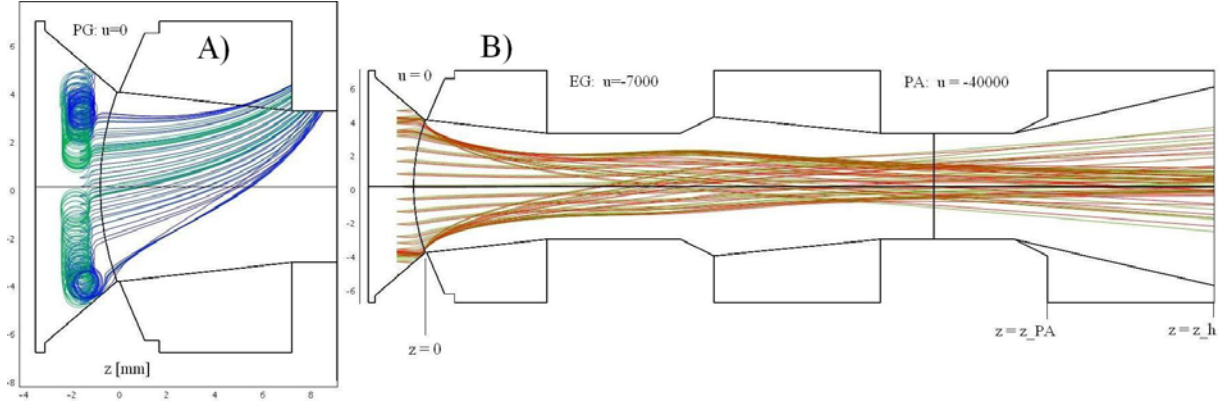


Figure 3: A simulation example (acceleration gap shorter than in NIO1, extraction voltage and bending fields are slightly lower); A) electrons; B)  $H^-$  ions; note the crossover of rays starting near the PG edge and the resulting halo.

In general  $N_n$  and  $N_e$  are complicated functionals of  $\phi$  and the plasma parameters, so that ray tracing seems necessary [4, 14, 15, 16]. Ray map interpolation was used in a self consistent code for Poisson-Vlasov solution, discussed elsewhere [17]. This code still consists of macros in a multiphysics environment [13], so flexibility to incorporate new effects is maximal. It was convenient to scale densities as  $n = N/N_0$ , with  $N_0$  the plasma density of negative charges much before the extraction, and to scale the potential as  $u = -(\phi - \phi_{PG})/(T_c)$ , where  $T_c$  is the temperature of the extraction plasma. Since  $T_e \cong 1$  eV there and  $N_0 \cong 3 \times 10^{17} \text{ m}^{-3}$ , collisional effects are strong and ion temperature  $T_p$  must be of the same order  $T_e \cong T_p \cong T_c$ . Poisson equation becomes

$$\Delta u = [n_p - n_n - u_e]/\lambda_D^2 \quad (3)$$

where the  $\lambda_D = (\epsilon_0 T_e / N_0 e^2)^{1/2}$  is the Debye length.

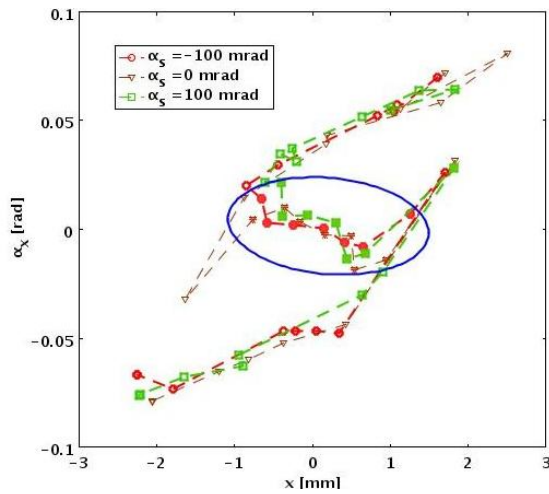


Figure 4:  $H^-$  phase space  $x, \alpha_x$  at  $z = 43$  mm with  $u_{EG} = -6900$ ;  $\alpha_s$  is the angular deviation at start. The halo rays (open markers) were started with a much closer spacing, which explains their lower weight in computing the emittance ellipse.

Expression of  $n$  in terms of  $u$  and the current modulus  $j_\Sigma(z, x)$  determined by ray map interpolation were discussed elsewhere [17]; here  $z$  is the beam extraction axis,  $y$  is the direction of an externally applied magnetic field, and the electrode structure is assumed periodic in  $x$ ; period  $L_x$  is the spacing between beamlets.

Sample results are shown in Figs. 3 and 4, with  $j(H^-) = 300 \text{ A/m}^2$  at the source. Thus  $N_0 = 3 \times 10^{17} \text{ m}^{-3}$ . Since  $\lambda_D = 0.014$  mm mesh be must be really dense in the plasma and 330000 degrees of freedom were needed in this example. Computer resources usage was reasonable: four ray tracing iterations were completed in 18 minutes, using 4 GB RAM and 7 CPU cores (total CPU time 5500 s). The simulation domain necessarily ends at a given  $z_h$ , after the end  $z_{pa}$  of the PA electrode; here  $z_h = z_{pa} + d_h$  with  $d_h$  mm the drift space. It must be discussed how  $d_h$  should be chosen: clearly it must be much greater than the length  $d_c$  needed to reach a compensation of the negative beam space charge; that is, for  $z > z_h$  the beam charge compensation should be at equilibrium.

From 1D equilibrium analysis [18] it is well known that space charge compensation of a negative ion beam is a fast process, which may reach a large fraction  $f_c$  of charge compensation; for example at a  $H_2$  pressure of 0.05 Pa and a beam voltage  $V_b = 60$  kV,  $f_c$  ranges from 0.997 (for a typical beam density  $N_b = 10^{15} \text{ m}^{-3}$  and a beam radius  $r_b = 4$  mm) to 1.0001 (for a beam density  $N_b = 10^{16} \text{ m}^{-3}$  and a beam radius  $r_b = 40$  mm). So  $d_h = 10$  mm seems provisionally reasonable. Another issue is that boundary conditions at  $z = z_h$  affects space charge compensation. To fix ideas, assume that drift tube has a radius  $R_{dr} = 50$  mm (much larger than  $L_x$ ) so that a general solution of Poisson equation for  $z > z_h$  is about

$$u(z, r) \cong A + B J_0(kr) e^{-kz} + C g(r/r_b) \quad (4)$$

where  $r = (x^2 + y^2)$  and  $k = 2.40483/R_{dr}$  and all modes but the fundamental with amplitude  $B$  were neglected; moreover  $C$  is the effect of the residual space charge and  $g$  is a shape function, depending on charge distribution inside the beam and about  $g = \ln(r/r_b)$  for  $r > r_b$ . Neglecting

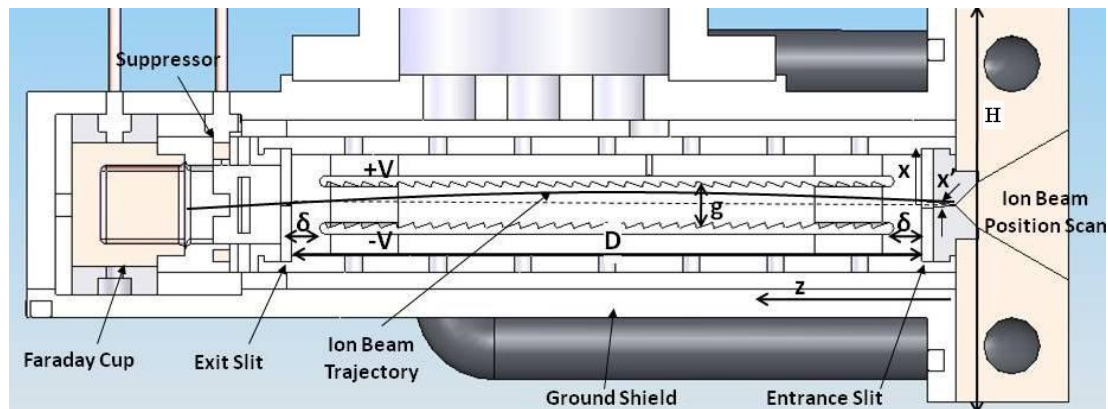


Figure 5: Typical scheme of an Allison meter measuring head, of height  $H$ ; secondary emission suppression is used; electrode parameters described in the text.

$C$  since the charge compensation is large, gives  $A = u_{dr}$ ; eliminating  $B$  gives the mixed boundary condition

$$u_{,z} = -k(u - u_{dr}) \quad (5)$$

which is easily implemented in the multiphysics solver[13]. In planar geometry, replace with  $k = \pi/2/R_{dr}$ . The case  $R_{dr} \rightarrow \infty$  is more elegant, gives a simple Neumann condition  $u_{,z} = 0$  and simplifies further analysis; practically it is often a good approximation (for a reasonable  $u_{dr}$ ).

## FAST EMITTANCE SCANNER

Over the last 20 years, Allison scanners [19, 20] have been introduced in many laboratories to measure the emittance of low-energy ion beams. Allison scanners feature entrance and exit slits that are rigidly mounted on the same support base, thus allowing for their relative alignment within tight tolerances. The space between the slits is occupied by a set of electric deflection plates as shown in Fig. 5. Charged particles that pass both slits are collected in the Faraday cup (FC), which features secondary electron suppression. A grounded shield surrounds the assembly, intercepting any charged particles that could produce ghost signals [21]. A stepper motor moves the entire assembly through the beam to probe the different positions of the beam. At each stop, the beam part that passed the entrance slit is scanned electrically across the exit slit to determine the distribution of the entry angles.

After passing the entrance slits, ions with energy  $eV_b$  enter the electric field between the deflection plates, which are charged to opposite voltages  $-V$  and  $+V$ . Before and after the opposite ends of the deflection plate the two selection slits are placed at an equal distance  $\delta$ ; the first slit selects the ion position, the second the ion angle. Let  $D$  be the distance between these slits. The deflection voltage-to-entrance-angle conversion depends primarily on lengths  $D$  and  $\delta$  and the gap  $g$  between the deflection plates. Making the assumption that electric field is uniform in the region inside plates of length  $D_\delta = D - 2\delta$  and falls to zero outside (hard edge approximation), the entry angle  $x'$  is related

to the voltage difference  $V_d$  between the deflection plates by  $x' = V_d D_\delta / (4gV_b)$ . The space between the deflection plates allows only for trajectories where  $x$  never exceeds  $g/2$ , which geometrically limits the angular acceptance to  $x'_M = \pm 2g/(D + 2\delta)$  where we took into account that trajectory is a parabola in the region between plates and a straight line outside. Correspondingly the maximum required voltage difference is

$$V_M = \pm \frac{8g^2 V_b}{D_\delta (D + 2\delta)} = \pm 2 \frac{(D + 2\delta)}{D_\delta} V_b x'_M{}^2 \quad (6)$$

We have chosen the front and rear slit width  $s$  to be equal to maximize the scanner current for a given angular resolution. Then the mechanical angular resolution is  $\theta_d = \pm s/D$ , which corresponds to a rms value (for a parallel beam uniformly illuminating the front slit)  $\theta_{rms} = s/(6^{1/2}D)$ . The FC signal current  $i_d$  is estimated from the ratio of scanner acceptance to the un-normalized phase-space area  $\pi\epsilon/\beta$ , so that  $i_d = I_b s^2 / [D(\pi\epsilon/\beta)]$ . Due to the finite bandwidth  $f$  of the Faraday cup amplifier, the smaller

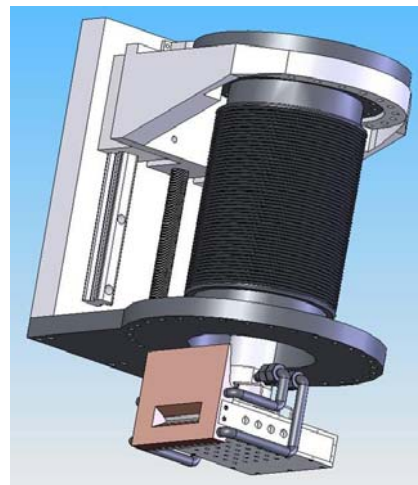


Figure 6: Artist view of the Allison scanner plugin module, in the beam-non-intercepting position.

Table 1: Beam Parameters for Scanner Specifications

	Units	NIO1	TRIPS
Beam ion		H <sup>-</sup>	H <sup>+</sup>
Energy $eV_b$	keV	60	80
Current $I_b$	mA	130	50
Power density	MW/m <sup>2</sup>	20.3	22.6
Beam dimension	mm	±40	±40
Beam divergence	mrad	±40	±130
Power (CW)	kW	7.8	4.0

rms observable is  $\theta_{rms} = 2^{1/2}x'_M/(\pi T f)$ , where  $T$  is the ramp time to analyze angles in the range  $\pm x'_M$ . By equating the full mechanical resolution with that due to the finite bandwidth, we obtain a criteria for the amplifier bandwidth  $f = 12^{1/2}x'_M D/(\pi s T)$ .

The beam part selected with the first slit expand itself due to finite emittance and due to space charge effects. It is important that space charge forces do not affect angular resolution; this implies a limit for the slit distance  $D$ . Consider a uniform elliptical beam with dimensions  $R_x$  and  $R_y$ . If we require that expansion due to space charge to be less than  $s/2$ , then  $D^2 < 2\pi\epsilon_0 R_x R_y m v_b^3 / (I_b e)$  with  $v_b$  the beam velocity; we get  $D < 0.35$  m.

In our work, we want to use the scanner for both NIO1 and TRIPS source. Currents, beam power and maximum beam divergence are different for the two sources (Table 1). Allison scanner has to be designed for the worst parameters. This means that we need a divergence acceptance of more than 130 mrad and dictates a relationship between  $g$ ,  $D$  and  $\delta$ . For economic reasons we choose a voltage range of  $\pm 2$  kV for deflection plates amplifier. Parameters of this new Fast Emittance Scanner (FES) are presented in Table 2. The scanner has 90 mm long deflection plates with a 8 mm gap centered between the slits separated by 100 mm. Accordingly, its geometrical acceptance is 145 mrad. Both deflection plates are powered with bipolar  $\pm 2$  kV voltage amplifiers. This limits the voltage acceptance to 188 or 141 mrad for ion source potentials of 60 or 80 kV, respectively.

The scanner is covered with a drilled aluminum shield that should guarantee a sufficient vacuum pumping. Getter pump may also be inserted. A very good heat removal is obtained by using aluminum nitride as electric insulator

Table 2: FES Design Parameters

	Units	NIO1	TRIPS	FES
$g$	mm	8	8	8
$D$	mm	100	100	100
$\delta$	mm	5	5	5
$s$	mm	0.05	0.05	0.05
$V_M$	kV	±0.43	±1.85	±2
$x'_M$	mrad	±40	±130	±145
$\theta_d$	mrad	±0.5	±0.5	±0.5
Slew rate	V/μs	300	300	300
$v_h$	m/s	0.3	0.3	0.3
$f$ bandwidth	MHz	31	23.3	35

material. The suppressor voltage will be tested by tuning the setup for maximum beam current in the Faraday cup of the scanner. For low suppressor voltages the Faraday cup current should change substantially. Then, to assure the suppression of all secondary electrons, the Faraday cup current has to reach a plateau significantly before reaching the intended suppressor voltage. Deflection plates have a sawtooth inner surface, to partly capture the secondary particle emission there produced by the ion impact. Provided that sawtooth depth is small enough, uniform field approximation is adequate, as easily shown by simulations. Some more elaborate machining of the deflection plates which may improve the secondary trapping efficiency is also being evaluated.

FES can work in two different modes: a very fast scan favored by an extremely fast motion (with velocity  $v_h$  up to 30 cm/s) of the active box through the beam and a slow scan (this is allowed by the efficient water cooling system) that guarantees a better resolution. An artistic view of the Fast Emittance Scanner is presented in Fig. 6.

## REFERENCES

- [1] A. T. Forrester, *Large Ion Beams*, John Wiley, NY, 1996.
- [2] H.P.L. de Esch et al., *Rev. Sci. Instrum.*, **73**, 1045 (2002).
- [3] R. S. Hemsworth, *Nuclear Fusion*, **43**, 851 (2003).
- [4] R. F. Welton et al., *Rev. Sci. Instrum.*, **75**, 1789 (2004).
- [5] P. Garin, Proceedings of EPAC08, Genoa, Italy, p 974 (2008).
- [6] M. A. Lieberman, A. J. Lichtenberg, *Principles of Plasma Discharges and Material Processing*, J. Wiley, NY, 1994.
- [7] M. Bacal, *Rev. Sci. Instrum.*, **79**, 02A516 (2008).
- [8] K. W. Ehlers, K. N. Leung, *Rev. Sci. Instrum.*, **52**, 1452 (1981).
- [9] L. Celona et al. *Rev. Sci. Instrum.*, **75**, 1423 (2004).
- [10] R. Gobin et al. *Rev. Sci. Instrum.*, **73**, 923 (2002).
- [11] M. Cavenago et al., in *Negative ions, Beams and Sources* (eds. E. Surrey, A. Simonin, AIP-CP 925), p 149 (2008)
- [12] L. Tonks, I. Langmuir, *Phys. Rev.*, **34**, 826, (1929).
- [13] *Comsol Multiphysics 3.3*, see also <http://www.comsol.eu>
- [14] P. Spadtke, *Rev. Sci. Instrum.*, **75**, 1643 (2004)
- [15] R. Becker, *Rev. Sci. Instrum.*, **75**, 1723, (2004).
- [16] G. Fubiani, H. P. L. de Esch, A. Simonin, R. Hemsworth, *Phys. Rev. ST-AB*, **11**, 014202 (2008).
- [17] M. Cavenago, P. Veltri, F. Sattin, G. Serianni, V. Antoni, *IEEE Trans. on Plasma Sci.*, **36**, 1581, (2008).
- [18] A. T. Holmes, *Beam Transport*, in *The Physics and Technology of Ion Sources*, (ed. I.G. Brown), J. Wiley, NY, 1989.
- [19] P. W. Allison, J. D. Sherman, and D. B. Holtkamp, *IEEE Trans. Nucl. Sci.*, NS-30, 2204-2206 (1983).
- [20] R. McAdams et al., *Rev. Sci. Instrum.*, **59**, 895 (1988).
- [21] M. P. Stockli et al., in Proc. of the 16th Int. Work. on ECR I. S., (ed. M. Leitner, AIP Conference Proceedings AIP-CP 749, Melville, New York) p 108 (2008).